Modelling coupled turbulence – Dissolved oxygen dynamics near the sediment–water interface under wind waves and sea swell

Mathieu Chatelain, Katell Guizien

Modelling coupled turbulence - dissolved oxygen dynamics near the sediment-water interface under wind waves and sea swell

Mathieu Chatelain[1,2,*] Katell Guizien[1,2]

[1] CNRS, UMR 7621, LOBB, Observatoire Océanologique,
F-66651, Banyuls/mer, France
[2] UPMC Univ Paris 06, UMR 7621, LOBB, Observatoire Océanologique,
F-66651, Banyuls/mer, France

*Corresponding author. Tel: +33 (0)468 887 394; Fax: +33 (0)468 887 395;
E-mail address: chatelain@obs-banyuls.fr

Abstract

A one-dimensional vertical unsteady numerical model for diffusion-consumption of dissolved oxygen (DO) above and below the sediment-water interface was developed to investigate DO profile dynamics under wind waves and sea swell (high-frequency oscillatory flows with periods ranging from 2 to 30 s). We tested a new approach to modeling DO profiles that coupled an oscillatory turbulent bottom boundary layer model with a Michaelis-Menten based consumption model.

The flow regime controls both the mean value and the fluctuations of the oxygen mass transfer efficiency during a wave cycle, as expressed by the non-dimensional Sherwood number defined with maximum shear velocity (Sh). The Sherwood number was found to be non-dependent on sediment biogeochemical activity (μ). In the laminar regime, both cycle-averaged and variance of the Sherwood number are very low ($\overline{Sh} < 0.05$, VAR(Sh) < 0.1 %). In the turbulent regime, the cycle-averaged Sherwood number is larger ($\overline{Sh} \approx 0.2$). The Sherwood number also has intra-wave cycle fluctuations that increase with the period and maximum shear velocity (VAR(Sh) up to 30 %). Our computations show that DO mass transfer efficiency under high-frequency oscillatory flows in the turbulent regime are water-side controlled by: (a) the diffusion time across the diffusive boundary layer and (b) diffusive boundary layer dynamics during a wave cycle. As a result of these two processes, when the wave period decreases, the Sh minimum increases and the Sh maximum decreases. Thus $\overline{Sh}$ values vary little, ranging from 0.17 to 0.23. For periods up to 30 s, oxygen penetration depth into the sediment did not show any intra-wave fluctuations. Values for the laminar regime are small ($\leq$ 1 mm for μ=2000 g m^{-3} d^{-1}) and decrease when the flow period increases. In the turbulent regime, the oxygen penetration depth reaches values up to five times larger than those in the laminar regime, becoming asymptotic as the maximum shear velocity increases.

Keywords: wave boundary layer - mass transfer - turbulent diffusion - unsteady flow - sediment diagenesis

1 Introduction

Diffusional mass transfer between bottom sediments and overlying water constitutes an essential coupling for benthic and pelagic ecosystems (Boudreau and Jørgensen, 2001). Transfer of oxygen across the sediment-water interface (SWI) regulates biological and geochemical processes of organic matter degradation in the upper sediment. Vertical oxygen mass transfers at the benthic or bottom boundary layer occur in a zone where gradients in physical, chemical and biological properties are sharp. In the water column, solute transport is dominated by turbulent mixing, except within the diffusive boundary layer (DBL) where turbulence diffusivity becomes negligible compared to oxygen molecular diffusion (Gundersen and Jørgensen, 1990). The thickness of the DBL regulates the kinetics of oxygen supply to the benthic organisms: while a thick DBL associated with small steady flow velocities (laminar regime) may be limiting for organisms with high oxygen uptake rates, a thin DBL associated with large steady flow velocities (turbulent regime) results in the highest possible oxygenation (Nakamura and Stefan, 1994; Hondzo, 1998; Steinberger and Hondzo, 1999). In nature, flows are generally turbulent with DBL thicknesses on the order 1–2 mm (Jørgensen and Revsbech, 1985) but they are also more often unsteady. As a consequence, the DBL thickness will fluctuate inducing oxygen profile dynamics (Jørgensen and Des Marais, 1990; Glud et al., 2007). Yet, such dynamics are not instantaneously responding to the hydrodynamic forcing. Transient oxygen profiles were observed in sediment cores immediately after stirring was stopped (Lohse et al., 1996). Numerical simulations have shown that the duration of the transitory regime between two steady states (with and without flow) decreases as both oxygen consumption and flow velocity increase (Higashino et al., 2004).

Amongst unsteady flows, oscillatory flows are of particular interest for the diffusion-consumption of oxygen at the SWI. Periodic flows are frequent in nature as they are linked to surface gravity waves. In the oceans, such flows are the most energetic (Massel, 1996) and they often destabilize the SWI in the nearshore zone (Harris and Coleman, 1998). Surface gravity wave energy is equally distributed between two types characterized by their period: wind waves and swell (periods from 2 to 30 s) and the diurnal and semi-diurnal tides (periods from 12 to 24 h). In lakes and lagoons, the period range for surface gravity waves is generally restricted to wind waves (period < 8 s) due to fetch limitations. But other types of oscillatory flows like a seiche with even longer periods (depending on the basin lengthscale and stratification) can be observed (Proudman, 1953). In 2003, the oxygen profile dynamics linked to periodic bottom layer turbulence under low-frequency waves (lake internal seiching with period of 18 hours) was observed for the first time (Lorke et al., 2003). Additionally, the effect of periodic flows (periods ranging from minutes to hours) on oxygen diffusion in the water column was investigated by numerical simulations (Higashino et al., 2003).

The present study examines the effect of wind waves and sea swell (periods ranging from 2 to 30 s) on oxygen diffusion and consumption at the SWI. Oscillatory flows exhibiting large velocity fluctuations from zero (at flow reversal) to a maximum value (orbital velocity) are associated with these high-frequency gravity waves (Airy, 1845). Near the bed, an oscillatory bottom boundary layer develops which exhibits strong turbulence dynamics with flow relaminarisation around reversal (Jensen et al., 2006) and consequently, large DBL thickness fluctuations at the flow periodicity. Under oscillatory flows, the oxygen concentration distribution dynamics may result not only from the DBL thickness value, but also from its dynamics as well. Hence, a new one-dimensional vertical, unsteady numerical model for diffusion-consumption of dissolved oxygen (DO) above and below the SWI was driven by the turbulent diffusivity associated with the wave bottom boundary layer modelled by Guizien et al. (2003). Wind waves and sea swell were described by idealized monochromatic waves to assess the respective influence of the wave period and orbital velocity. The new model was used to examine three fundamental questions about the dynamics of DO distribution under high-frequency waves. First, what are the characteristic time scales of the forcing that drive the intra-wave dynamics of DO ? Second, how does the DO mass transfer vary with the wave period and the orbital velocity (mean value and fluctuations during a wave cycle) ? And third, to what extent do wind waves and sea swell drive sediment oxygenation (DO penetration depth) ?

2 Material and methods

2.1 Model formulation

Dissolved oxygen traverses two diffusive boundary layers from the water column into the sediment. The first layer is in the water immediately above the sediment, and the second is in the sediment immediately below the sediment-water interface (Fig. 1).

[Figure 1]

A one-dimensional vertical (1DV) numerical model of the DO balance in water and sediment is proposed. For the sake of simplicity, we assume a constant porosity of the sediment. Advection due to permeability, bioturbation and bioirrigation in the sediment is neglected. Microbial organic matter degradation occurring in the sediment is taken into account, as well as chemical reactions involving oxygen consumption. Both are modelled by Michaelis-Menten consumption kinetics (House, 2003). Such a mathematical formulation allows a constant consumption when the DO concentration is large (*i.e.* non limiting, zero-order kinetics) and a decreasing consumption when DO concentration approaches zero (first-order kinetics). This formulation is thus consistent with both zero flux and concentration for DO at the lower boundary condition deep in the sediment. Moreover, prescribing a constant consumption near the interface assumes that neither acclimatization nor growth of the respiring community occurs inside a wave cycle. Finally, it is assumed that oxygen consumption can be neglected in the water column. Thus we define:

$$\frac{\partial C^*}{\partial t^*} = \frac{\partial}{\partial z^*}\left(D^* \frac{\partial C^*}{\partial z^*}\right) - \alpha . \frac{\mu^* C^*}{K^*_{O_2} + C^*} \tag{1}$$

where the non-dimensional parameters are

$$C^* = \frac{C}{C_0}, t^* = \frac{\nu t}{h^2}, z^* = \frac{z}{h}, D^* = \frac{D}{\nu}, \mu^* = \frac{\mu h^2}{\nu C_0}, {K_{O_2}}^* = \frac{K_{O_2}}{C_0}. \tag{2}$$

C is the DO concentration, t is time, z is the vertical coordinate (positive upward), D is the vertical diffusivity, μ is the maximum oxidation rate, K_{O_2} is the oxygen half-saturation constant, and α is a numerical constant (α=1 in sediment and α=0 in water). Reference values are ν the kinematic viscosity in water, C_0 the bulk water concentration, and h a length greater than the sum of DBL thickness in water and DO penetration depth in sediment.

In sediment, oxygen vertical diffusivity D is equal to the effective diffusivity D_s, which is molecular diffusion corrected for tortuosity. It can be expressed, through Archie's law, as a function of molecular diffusivity and porosity of the sediments (Ullman and Aller, 1982):

$$D_s = \phi^{m-1}\ D_w \tag{3}$$

where ϕ is the porosity, and m denotes an exponent corresponding to different kinds of sediment (m=3, Manheim and Waterman, 1974). Molecular diffusion D_w for oxygen is assumed constant, using a Schmidt number $Sc=\nu/D_w$=500 at 20^{o}C (Denny, 1993).

In water, oxygen vertical diffusivity D is the sum of molecular (D_w) and turbulent (D_t) diffusivities. Using the analogy between momentum and mass transfer, the turbulent diffusivity (D_t) is assumed to be equal to the eddy viscosity (ν_t) in water. The model formulation thus allows time-variations of turbulent diffusivity to account for unsteady hydrodynamics.

Equation (1) is solved using the implicit finite control volume method of Patankar (1980). The spatial computational domain went from $-h_s$ in the sediment, to h_w in the water column ($h = h_s + h_w$). Two exponential grids were defined with n_s points in sediment and n_w points in water. Each mesh starts at z=0, reading:

$$|z_{i+1} - z_i| = dz_i = s\ r^i \tag{4}$$

taking (r,s) equals (r_s,s_s) in sediment and (r_w,s_w) in water. The SWI is the first sediment point, located at z=0 (α=1, $D = D_s$). This grid was adopted because it is well adapted to refining the nearbed description of each domain where gradients are sharp. Meshing independence of the computations was studied and showed insensitivity of the results for a resolution that yields r_s=1.054, s_s=1×10^{-5} (n_s=194) and r_w=1.054, s_w=1×10^{-7} (n_w=320) for sediment and water, respectively (in Eq. 4).

Boundary conditions for DO concentration are imposed at the top and the bottom of the calculation domain:

$$\begin{cases} C^* = 0 & \text{at } z^* = -h_s/h \\ C^* = 1 & \text{at } z^* = h_w/h \end{cases} \quad (5)$$

The first condition expresses that all DO reaching the sediment should be utilized within the oxygen penetration depth. The second indicates that at the upper limit of the computational domain the water column is fully mixed and the oxygen concentration equals the bulk water concentration. Bulk DO concentration was arbitrarily set to 10 g m^{-3} (Glud et al., 2003).

As we are dealing with periodic hydrodynamic forcing, a finite number of time steps (n_t=360) is required to define an entire period cycle, and periodic boundary conditions are applied stating $C^*(z,n_t+1)=C^*(z,1)$. The equilibrium solution is the solution when the maximum DO concentration difference at the same phase during two consecutive cycles was less than a convergence criterion ϵ. We used $\epsilon=10^{-8}$ as the convergence criterion.

2.2 Sediment characteristics and hydrodynamic forcing

This study examines the nearbed dynamics of oxygen mass transfer transport under wave forcing over a smooth bottom, as can be observed in shallow estuaries open to the sea. Porous silty sediment conditions were used (median diameter d_{50}=0.002 cm; bottom roughness k_n=0.005 cm; porosity ϕ = 0.9). The half-saturation constant for DO is set to a constant value (K_{O_2}=0.2 g m^{-3}, Hao et al., 1983). Two biogeochemical activities were tested: high oxidation rate (μ=2000 g m^{-3} d^{-1}) and low oxidation rate (μ=50 g m^{-3} d^{-1}, Higashino et al., 2004). These values correspond to oxygen consumption times in the sediment of 422 s and 4.8 h, respectively.

A linear wave forcing is considered:

$$U(t) = U_w \sin\left(\frac{2\pi t}{T}\right) \quad (6)$$

where T is the leading wave period and U_w is the nearbed orbital velocity.

In order to investigate the effect of oscillating flows typical of wind waves to swell on DO uptake dynamics, we considered wave orbital velocities ranging from 20 to 200 cm s^{-1} and periods ranging from 2 to 30 s. Virtually, any orbital velocity / period couple can be considered, provided the wave stability criterion is fullfilled. We excluded some orbital velocity / period couples which are unrealistic as they would correspond to unstable breaking waves. Using a breaking-wave criterion of $H < 0.8\ D$ (where H is the wave height and D is the water depth), the orbital velocity restrictions only applied to waves with periods shorter than 4 s.

Hydrodynamic forcing for the DO model consisted of time-varying eddy viscosity profiles $\nu_t(z,t)$ in the wave boundary layer during a wave cycle. Together with bottom shear stress time series, these were computed using a 1DV bottom boundary layer numerical model dedicated to periodic flow (Guizien et al., 2003), given the bottom roughness k_n. The shear velocity u^* at the bed is then:

$$u^*(t) = \sqrt{\frac{\tau(t)}{\rho}} \quad (7)$$

where ρ denotes the water density.

[Figure 2]

Fig. 2 shows the time evolution during a wave cycle of the shear velocity $u^*(t)$ for two contrasted wave orbital velocities at the same wave period (T=15 s) to illustrate the laminar and turbulent regime. In both regimes, during each half of a wave cycle, shear velocity varies from nearly zero to a maximum u^*_m (not a sine form). As typically seen in oscillatory flows, the shear velocity maximum and minimum are ahead of the wave velocity outside the boundary layer, showing that small velocities (near the bottom) reverse more easily than larger ones (far from the bottom) when the pressure gradient reverses. This phase shift decreases from 45^o in the laminar case to about 10^o in the fully turbulent regime (Fredsøe and Deigaard, 1992). For the same reason, turbulent diffusivity (not shown) exhibits a phase shift with the outer flow velocity which varies across the boundary layer. A laminar regime is defined as a wave period and an orbital velocity for which the phase shift is 45^o. It corresponds in our computations to a wave Reynolds number below 320:

$$Re_\delta = \frac{U_w \delta}{\nu} \tag{8}$$

with $\delta = \sqrt{\nu T/\pi}$ the wave viscous boundary layer height (Vittori and Verzicco, 1998). In the turbulent regime, the shear velocity time evolution jumps during the acceleration phase, marking the onset of turbulence that occurs after the boundary layer relaminarisation around flow reversal (Jensen et al., 2006). In the laminar regime, such a jump is absent (flow remains laminar during the entire wave cycle). The laminar regime ($Re_\delta \leq 320$) is shown in light grey on Fig. 3. For the wave climates that were investigated, maximum shear velocities ranged from less than 1 to 8 cm s^{-1}. The sensitivity to the wave period is accentuated when the period is small. The dark grey area indicates breaking wave values on the same figure.

[Figure 3]

Fig. 4 displays computed turbulent diffusivity (*i.e.* eddy viscosity) profiles every 30^o along half a wave cycle in the turbulent regime. Temporal changes in D_t values reflect the temporal variations during a wave cycle of the viscous sublayer thickness $\delta_\nu(t)$ (the area where $D_t < \nu = 10^{-2}$ cm^2 s^{-1}). Consequently, the oxygen DBL thickness $\delta_D(t)$ (the area where $D_t < D_w = 2\times10^{-5}$ cm^2 s^{-1}) also shows temporal variations during a wave cycle, ranging from around 5×10^{-3} to 3×10^{-2} cm for T=25 s and U_w=120 cm s^{-1} (u^*_m=5 cm s^{-1}). It should be noted that the exponential mesh creates a coarser resolution in $\delta_D(t)$ computations for large DBL thicknesses.

[Figure 4]

2.3 Model analysis

Computational results consisted of DO vertical profiles at different phases during a wave cycle. For each DO profile, we defined the interfacial concentration $C_w(t)$, the penetration depth $\delta_s(t)$ (with $C^*(z{=}\delta_s(t))$=0.001) and the dissolved oxygen uptake (DOU) at the SWI (Fig. 1). The latter is evaluated from Fick's first law of diffusion (Berner, 1980):

$$DOU(t) = -D_w \frac{\partial C}{\partial z} = -\frac{D_w C_0}{\beta(t)}. \tag{9}$$

Practically, the instantaneous DOU(t) is computed taking the slope $\beta(t)$ of the DO vertical profile over the three first grid points in water, which height is always much smaller than the DBL thickness. The dimensionless Sherwood number, Sh, is introduced, following Higashino et al. (2003):

$$Sh(t) = \frac{DOU(t)\ Sc}{u^*_m\,(C_w(t) - C_0)} \tag{10}$$

where u^*_m is the maximum shear velocity. The Sherwood number can be interpreted as a ratio between the effective oxygen transfer rate and turbulent diffusion rate. It thus measures the turbulence efficiency to supply oxygen to the sediment. Following Lorke et al. (2003), we defined a time scale $t_D(t)$ for the oxygen diffusion across the DBL as:

$$t_D(t) = \frac{\delta_D(t)^2}{D_w}. \tag{11}$$

All these time-varying quantities are described by their mean value (indicated by the overline notation) and their variance (VAR(x)=100×RMS(x)/$\overline{x}$ in %, where RMS is Root Mean Square) during a wave cycle.

To go further, a time scale (t_w) describing the temporal dynamics of the DBL thickness is introduced:

$$t_w(t) = \frac{\delta_D(t)}{|\frac{\partial \delta_D}{\partial t}|}. \tag{12}$$

This time scale describing the intra-wave DBL dynamics should be compared to the time scale for the establishment of a local DBL. Similar reasoning was adopted by Lorke et al. (2003), where the authors compared relative importance of vertical diffusion versus horizontal advection. When $t_w(t)$ is larger than $t_D(t)$, the DBL thickness varies less rapidly than the time required for the DBL to establish: diffusive

fluxes will follow the local DBL thickness fluctuations. Conversely when $t_w(t)$ is smaller than $t_D(t)$, the DBL thickness varies more rapidly than the time required for the DBL to establish: transient diffusive fluxes corresponding to average DBL thickness over the period are simulated.

3 Results

3.1 Intra-wave cycle dynamics

In the laminar regime (shear velocity time series shown on Fig. 2 for T=15 s, U_w=10 cm s^{-1}, u^*_m=0.8 cm s^{-1}, Re_δ=218), the time required by oxygen to diffuse through the DBL (t_D) during the wave cycle was very large ($\approx$ 1.1 days) compared to both the oxygen consumption time in the sediment (t_c) and the wave period (T). The values of t_D were also fairly constant during the wave cycle (data not shown). Consequently, both DOU and concentration at the SWI displayed very small and constant values (DOU=0.12 g m^{-2} d^{-1}, C_w=0.01 C_0). The oxygen penetration depth was also very small (δ_s=0.03 cm). When $t_D \gg t_c$, oxygen is consumed more rapidly in the sediment than it diffuses from water into the sediment: SWI oxygenation is limited by the transfer time through the water DBL.

In the turbulent regime, the time required by oxygen to diffuse through the DBL (t_D) is much shorter than in the laminar regime, and reaches lower values than oxygen consumption time in the sediment (t_c). Figure 5 shows the dynamics during a wave cycle of the parameters u^*, t_D, DOU and C_w/C_0 for a 15 s period wave with U_w=128 cm s^{-1} (u^*_m=5 cm s^{-1}, Re_δ=2797) and the highest oxygen consumption rate in the sediment (μ=2000 g m^{-3} d^{-1}, t_c=432 s). The oxygen diffusion time through the DBL (t_D) varied from less than 2 s to about 40 s during each half a wave cycle, with $\overline{t_D}$=10 s. SWI oxygenation is no longer limited by the transfer time through the DBL, resulting in a much higher DOU and interfacial concentration ($\overline{DOU}$=2.1 g m^{-2} d^{-1}, $\overline{C_w}$=0.86 C_0), and a higher penetration depth ($\overline{\delta_s}$=0.12 cm) compared to the laminar regime.

[Figure 5]

Values of t_D exhibited periodic fluctuations every half a wave cycle (Fig. 5b): it had a maximum around flow reversal and dropped rapidly at the onset of turbulence during flow acceleration. It decreased more gently until shear velocity reached a maximum (turbulent period labelled θ_1). As the shear velocity decreased, t_D increased slightly during the turbulent period labelled θ_2. Then it increased more rapidly as the bottom boundary layer became laminar during flow deceleration (relaminarization period labelled θ_3) to reach its maximum value again when the outer flow speed is zero. During θ_1 and θ_2, t_w is longer than t_D (bold line on Fig.5b) while during θ_3, t_w is shorter than t_D. While the t_D minimum occurs when the shear velocity is at a maximum, the t_D maximum occurs after the shear velocity minimum, close to the flow reversal point. This delay reflects the phase lagging of turbulent diffusivity across the bottom boundary layer. As a consequence of the t_D fluctuations, DO concentrations at the SWI also displayed intra-wave dynamics: the DOU at the SWI varied between a minimum and maximum value during each half wave cycle, yielding VAR(DOU)=14 % (Fig. 5c). The minimum value of the DOU occurs at the end of the relaminarization period θ_3. The DOU starts to increase at the laminar-turbulent transition when diffusion time had strongly decreased, reaches a maximum during the turbulent period, and then decreased until the next laminar-turbulent transition. It is noteworthy that during θ_3, the DOU decreases steadily without reflecting the large fluctuations of t_D around flow reversal. As a result of the DOU fluctuations, oxygen concentration at the SWI exhibited similar intra-wave fluctuations, although those were damped (VAR(C_w/C_0)=1 %, Fig. 5d) and delayed compared to the DOU fluctuations. Finally, the penetration depth did not display any intra-wave dynamics.

3.2 Effect of the wave period and orbital velocity

Fig. 6 shows the temporal evolutions of t_D, DOU and C_w/C_0 during a wave cycle for the same wave period (T=15 s) and three orbital velocities (U_w=62, 128, 195 cm s^{-1}), which correspond to three maximum shear velocities (u^*_m=3, 5, 7 cm s^{-1} respectively) and three Reynolds numbers (Re_δ=1355, 2797, 4261 resp.). When the maximum shear velocity increases, the minimum value for t_D decreases from 5.3 to 0.7 s since the minimum DBL thickness is imposed by the maximum shear velocity. Moreover, the onset of turbulence occurs at an earlier phase during the accelerating phases of the wave cycle and the duration of period θ_1 increases. The duration of the relaminarization period θ_3 decreases from 5 to 2.6 s which limits the laminar DBL development around flow reversal. The maximum values for t_D around flow reversal decreases, although remaining larger than the wave period for the three cases

shown on Fig. 6a. As far as DOU is concerned (Fig. 6b), when the maximum shear velocity increases, the maximum value of the DOU increases while the minimum value of the DOU decreases, being phase locked to the laminar-turbulent transition. Besides, the maximum value of the DOU occurs at an earlier phase during the turbulent period. As a result, intra-wave fluctuations of DOU and oxygen concentration at the SWI (Fig. 6c) increase with the maximum shear velocity. Since the maximum DOU increased more than the minimum DOU, cycle-averaged values for DOU also tend to increase with the maximum shear velocity, although the values are close: $\overline{DOU}$ ranges from 1.99 to 2.16 g m^{-2} d^{-1}. Cycle-averaged values for the oxygen concentration at the SWI also increase when the shear velocity increases ($\overline{C_w}$=0.78, 0.86, 0.91 C_0 for u^*_m=3, 5, 7 cm s^{-1} respectively). It is interesting to note that while the C_w response to DOU fluctuations during a wave cycle is attenuated, its response to changes of cycle-averaged values of DOU is amplified.

[Figure 6]

Fig. 7 shows the temporal evolutions of t_D, DOU and C_w/C_0 during a wave cycle for the same maximum shear velocity (u^*_m=5 cm s^{-1}) and three wave periods (T=7, 12, 25 s), which correspond to three Reynolds numbers (Re_δ=1627, 2404, 3865 resp.). For the three periods, the oxygen diffusion time (t_D) reached the same minimum value when the shear velocity is maximum, which occurred around the same phase in the three cases: the minimum DBL thickness is imposed by the maximum shear velocity which is the same for the three cases depicted on Fig. 7a. However, as the period increases, not only the time between two flow reversal increases, but also the laminar-turbulent transition occurs at an earlier phase during the accelerating phases of the wave cycle. Consequently, the duration of the turbulent periods ($\theta_1 + \theta_2$) is increased in absolute values and also in proportion of the wave period. When the period increases, the duration of the relaminarization period θ_3 also increases from 2.2 to 5.1 s, which facilitates the relaminarization around flow reversal, yielding larger maximum values for t_D. However, in proportion of the wave period, the duration of the period θ_3 decreases when the wave period increases. Regarding the DOU (Fig. 7b), when the wave period increases, the maximum value of the DOU increases while the minimum value decreases. The fluctuations of DOU and C_w during the wave cycle (Fig. 7c) thus increase with the period. Although DOU cycle-averaged values vary little with the wave period ($\overline{DOU}$ ranging from 2.09 to 2.12 g m^{-2} d^{-1}), DOU exhibits the minimum value for T=12 s. Cycle-averaged values for the oxygen concentration at the SWI display the same pattern with amplification ($\overline{C_w}$=0.86, 0.85, 0.88 C_0 for T=7, 12 and 25 s respectively).

[Figure 7]

3.3 Trends in cycle-averaged DO quantities

A similar dependence for $\overline{DOU}$, VAR(DOU), $\overline{C_w}$ and VAR(C_w) on the wave characteristics was found for high (μ=2000 g m^{-3} d^{-1}) and low (μ=50 g m^{-3} d^{-1}) biogeochemical activities in the sediment. The non-dimensional Sherwood number defined by Eq. (10) was used to describe the DO mass transfer at the SWI. It also provides a measure of the hydrodynamic efficiency of this mass transfer: the larger the Sherwood number, the lower the maximum shear velocity for the higher oxygen transfer at the SWI. Since the Sherwood number was non-dependent on the biogeochemical activity of the sediment, it was used to summarize the dependency of the DO mass transfer at the SWI on the wave period and the orbital velocity (Fig. 8), and finally on the wave Reynolds number (Fig. **??**).

Laminar flow conditions ($Re_\delta \leq 320$ on Fig. **??** and light grey areas on Fig. 8) significantly hinder the transfer of dissolved oxygen and strongly reduce the presence of oxygen at the SWI, yielding very low non-dimensional mass transfer coefficients on average ($\overline{Sh} < 0.05$). Intra-wave cycle fluctuations are negligible (VAR(Sh) < 0.1 %, Figs. 8b and **??**b). When the wave boundary layer becomes turbulent ($Re_\delta > 320$), $\overline{DOU}$ and $\overline{C_w}$ displayed larger values than in the laminar regime (up to 2.15 g m^{-2} d^{-1} and 0.9 C_0). Over the range of wave conditions, $\overline{Sh}$ varied from 0.17 to 0.23, displaying minimum values for wave periods ranging from 10 to 15 s and orbital velocity ranging from 80 to 200 cm s^{-1} (Fig. 8a) corresponding to Reynolds numbers between 1500 and 3500 (Fig. **??**a). The Sherwood number fluctuations during a wave cycle increased with the wave period and orbital velocity (*i.e.* with the Reynolds number), yielding VAR(Sh)=30 % (as a result of VAR(DOU)=17 % and VAR(C_w)=1.75 %) for U_w=200 cm s^{-1} and T=30 s (Re_δ=6180).

[Figure 8]

Fig. 9 shows $\overline{DOU}$ and $\overline{C_w}/C_0$ versus the cycle-averaged (mean) shear velocity $\overline{u^*}$ during a wave cycle in the laminar and the turbulent regimes, and for two sediment biogeochemical activities. Whatever the flow regime, $\overline{DOU}$ is smaller and $\overline{C_w}/C_0$ is larger for the less active sediment (μ=50 g m^{-3} d^{-1}) than for the more active sediment. In the laminar regime, $\overline{DOU}$ and $\overline{C_w}/C_0$ increased linearly with the mean shear velocity up to 1.6 cm s^{-1}. In the turbulent regime, both quantities reached an asymptote for the largest mean shear velocity.

[Figure 9]

As far as the oxygen penetration depth is concerned, in the laminar regime, it decreased as the wave period increased, whatever the orbital velocity and for the two biogeochemical activities (Fig. 10a). The oxic layer is thin, ranging from 0.38 to 0.79 cm and from 0.02 to 0.06 cm for μ=50 and μ=2000 g m^{-3} d^{-1} respectively. When the overlying flow is turbulent, oxygen penetration depth is thicker and again strongly depends on the biogeochemical activity in the sediment (δ_s=1.03 and 0.15 cm for μ=50 and μ=2000 g m^{-3} d^{-1} respectively). However, in the turbulent regime, oxygen penetration depth no longer depends on the wave period and reaches an asymptote when shear velocity increases (Fig. 10b). For all the computations, DO penetration depth never showed intra-wave dynamics (*i.e.* VAR(δ_s)=0).

[Figure 10]

Finally, the convergence time (t_{st}) of DO profiles from an initial state (where C^*=1 in water and C^*=0 in sediment) to an equilibrium state was estimated from the calculations (data not shown). In the laminar regime, t_{st} scaled from around 20 to 108 h and from around 20 to 92 h when biogeochemical consumption was low (μ=50 g m^{-3} d^{-1}) and high (μ=2000 g m^{-3} d^{-1}), respectively). Time to reach equilibrium state is shorter when the flow is turbulent (less than 15 h). For the less active sediment, t_{st} varied little (between 11 and 13 h) with the wave period or orbital velocity. For the more active sediment, t_{st} ranged from 1 to 15 h, and fastest convergence was obtained for the higher Reynolds number.

4 Discussion

4.1 Characteristic time scales of non-steady DO dynamics under oscillatory flows

Our simulations showed that in the turbulent regime, the periodic fluctuations of the DBL thickness under oscillatory forcing induced periodic fluctuations of the DO concentration above and at the SWI. These fluctuations are not phase locked, evidence of transient adjustment to DBL thickness fluctuations. These features were previously observed on a lake internal seiching with a period of 18 hours (Lorke et al., 2003). Below the SWI, fluctuations are rapidly damped out. In the laminar regime, however, no fluctuations of the DO concentration were observed, even in the overlying water.

Three processes, all with different time scales, interplay during the wave period: (1) the oxygen consumption in the sediment, (2) the oxygen diffusion across the DBL, and (3) the DBL periodic dynamics. The relative importance of the first two processes was discussed by Higashino et al. (2004) for steady flows. In a laminar regime, the oxygen diffusion time across the DBL (t_D) is much larger than the oxygen consumption time in the sediment (t_c): SWI oxygenation is limited by the oxygen supply, leading to low values for the DOU and C_w. Conversely in a turbulent regime, the oxygen diffusion time across the DBL (t_D) is strongly reduced and SWI oxygenation is then scaled by the oxygen consumption in the sediment (t_c). In the case of unsteady wave forcing, the DBL periodicity whose time scale is the wave period (T) will interfere with the oxygen consumption and diffusion.

For high-frequency waves with periods up to 30 s, the sediment oxygen consumption time (t_c) will always remain longer than the wave period (T). Thus, any periodic fluctuation disappears rapidly in the sediment. In the turbulent regime, the oxygen diffusion time (t_D) can reach shorter values than the wave period (T): every half a wave period, the t_D value falls during the turbulent phases θ_1 and θ_2. Briefly put, the minimum value of t_D should be compared to the duration of the turbulent part of the wave cycle (Fig. **??**).

As the wave Reynolds number increases, the minimum value of t_D decreases and the duration of the turbulent phases increases (when $t_w > t_D$). DOU has then more time to adjust to the lower values of the minimum of t_D, and its intra-wave fluctuations grow. However, when the minimum value of t_D remains longer than the duration of the turbulent part of the wave cycle ($(\theta_1 + \theta_2)/\min(t_D)$,

$2050 < Re_\delta < 2500$ on Fig. **??**), the maximum value of the *DOU* will not have time to equilibrate with the low value of t_D. The maximum values of the Sherwood number are limited by the short duration of the turbulent phases. Consequently, intra-wave fluctuations are supported by the minimum values of the Sherwood number which decrease rapidly. Cycle-averaged value of the Sherwood number ($\overline{Sh}$) decreases. As the wave Reynolds number further increases, the minimum value of t_D decreases until reaching shorter values than the period θ_1 ($\theta_1/\min(t_D)$, $2800 < Re_\delta < 3300$ on Fig. **??**). The maximum value of the Sherwood number increases rapidly, following the decrease of the t_D minimum, while the minimum value of the Sherwood number is limited by the duration of the relaminarization period θ_3. Cycle-averaged value of the Sherwood number ($\overline{Sh}$) increases.

As a result of the competition between the oxygen diffusion time and the time granted to this rapid diffusion, $\overline{Sh}$ exhibits a minimum value for Re_δ between 2050 and 3300 (light gray area on Fig. **??**a), which corresponds to sea swell conditions ($10 < T < 15$ s and $80 < U_w < 200$ cm s^{-1}). In other words, some sea swells can be less efficient than wind waves (periods below 8 s) for oxygen mass transfer at the SWI.

4.2 Comparison with DO dynamics under steady flows

Previous experimental studies investigated the *DOU* dynamics under steady flows and showed an increase of the uptake with the flow shear velocity (Booij et al., 1994; Mackenthun and Stefan, 1998; Steinberger and Hondzo, 1999; Tengberg et al., 2004). These results were obtained for various sediment types (natural and artificial), but no indication of the sediment biogeochemical activities were given. Consequently, direct comparison of our results with previous published experimental work cannot be quantitative. However, qualitatively, our study confirm an increase of the *DOU* with the shear velocity. To our knowledge, the only study which can be used for a quantitative comparison is the numerical study by Higashino et al. (2004). *DOU* levels are quite similar, but the oxygenation at the interface is much greater in the case of steady flows. For $\overline{u^*}$=1 cm s^{-1} and μ=2000 g m^{-3} d^{-1}, oxygen transfer efficiency (*i.e.* Sherwood number) deduced from their calculations reaches Sh=0.36 whereas it reaches $\overline{Sh}$=0.25 in our study.

High-frequency waves are less efficient than steady current for the oxygen mass transfer at the SWI. Such finding should meanwhile be debiased by the occurrence frequency of each flow condition. Over the range of wave conditions we tested, the laminar regime corresponds to orbital velocities lower than 40 cm s^{-1} for the periods below 5 s and orbital velocities lower than 15 cm s^{-1} for periods up to 25 s. For the smallest periods corresponding to building wind waves (below 5 s), the wave height is also generally small and the laminar regime should be the most frequent regime in the bottom boundary layer, except in very shallow conditions (less than half a meter of water). This situation is likely to be encountered frequently in small closed basins (small lakes, lagoons, etc.).

As the wave period increases (when the wind fetch is larger), the laminar regime would become rarer: for instance, for a wave period of 8 s over 10 m water depth, the wave bottom boundary layer would be turbulent for a wave height H larger than 0.3 m, yielding $\overline{Sh}$=0.18. For H=1.6 m, orbital velocities reach 60 cm s^{-1} ($\overline{u^*}$=2.1 cm s^{-1}, $\overline{Sh}$=0.274), and yields on average a high SWI oxygenation ($\overline{C_w} \approx 0.8\ C_0$) due to large flux ($\overline{DOU} > 2$ g m^{-2} d^{-1}). Such wave conditions are frequently observed at sea (about 50 % of the time on the French Atlantic coast, Butel et al., 2002). After Higashino et al. (2004), reaching $C_w \approx 0.8\ C_0$ under a steady flow requires a lower oxygen flux $\overline{DOU}$=1.8 g m^{-2} d^{-1} associated with a lower shear velocity of 1.35 cm s^{-1}. Such steady shear velocity values correspond to a current speed of 30 cm s^{-1} at 1 m above a smooth bed. Even the most energetic tidal flow will not have such values more than 50 % of the time (Butel et al., 2002). Thus, it may be estimated that waves will promote a higher sediment oxygenation more frequently than steady currents. Additionally, DO profiles respond to the flow within a few hours. Even short events of wind waves or sea swell may notably stimulate shallow sediment oxygenation and oxygen exchange across the SWI.

4.3 Comparison with DO dynamics under low-frequency flows

Higashino et al. (2003) already attempted to describe the unsteady diffusional mass transfer under low-frequency periodic flows (periods ranging from 10 s to 10 h). Their numerical modelling was, however, restricted to the water column and they used a time varying water diffusivity derived from Dade (1993) steady-state parameterization. This may be valid for slowly varying flows, but not for high-frequency waves. Time scales of diffusion across the viscous sublayer are of the same order of magnitude as the wave period for high-frequency flows. As a consequence the turbulent shear stresses display

a phase lag across the boundary layer (Dohmen-Janssen, 1999) and the phase at which the laminar-turbulent transition occurs during each acceleration of the wave cycle depends on the wave Reynolds number Re_δ (Jensen et al., 2006). These features are well reproduced by the turbulent boundary layer model we used to compute the unsteady diffusive forcing (Guizien et al., 2003).

To a small extent, the results presented in this paper tally with previous calculations of the oxygen distribution dynamics under low-frequency flows (Higashino et al., 2003), as intra-wave fluctuations of the Sherwood number effectively tends to zero when the period becomes shorter. Nonetheless, regarding the cycle-averaged value of the Sherwood number, our results are in contradiction to the afore-mentionned study. Authors reported a decrease of the cycle-averaged Sherwood number with the flow period, while we demonstrated a more complex pattern depending on the flow period and orbital velocity as well ($\overline{Sh}$ is minimum around T=10-15 s and U_w=120-180 cm s^{-1}). This difference is simply explained by the dependence of the maximum value of the Sherwood number on the wave period which was lacking in Higashino et al. (2003) study. Only the intra-wave minimum value of the Sherwood number increased as the wave period decreased from 10 h to 10 s. Yet, we showed that the values of both the maximum and the minimum of the Sherwood number depend on the wave period (given a shear velocity maximum).

It should also be pointed out that our Sherwood number values ($\overline{Sh}$ around 0.2) are less than half of the values obtained by Higashino et al. (2003) for similar flow conditions ($\overline{Sh}$=0.5 for T=20 s, u^*_m=1 cm s^{-1}). The authors extrapolated their results to state that when the wave period tends to zero, the Sherwood number should approach a maximum corresponding to the Sherwood number value for steady-state conditions at the shear velocity maximum. Using the simulations from a study of the *DOU* dynamics under steady flows (Higashino et al., 2004), the upper limit of the Sherwood number under periodic flow (when the maximum shear velocity is u^*=1 cm s^{-1}) should be Sh=0.36. We argue that $\overline{Sh}$ values were overestimated by Higashino et al. (2003) probably because the interfacial oxygen concentration was assumed as a constant, while it was not in the present study.

4.4 Consequences for biological systems

Oxygen near the SWI is essential for both biological production and decomposition processes. Oxygen concentration is a regulating mechanism for benthic community complexity (Llansó, 1992), for regeneration of nutrients (Rahm and Svensson, 1989), and it also constrains chemical (Cai and Sayles, 1996) and biological (House, 2003) reactions. In a laminar regime, the transfer of DO is strongly impeded by the thickness of the DBL and hypoxic conditions ($C < 2$ ml l^{-1} $\approx$ 2.4 g m^{-3}, Diaz and Rosenberg, 1995) may appear near the SWI. A continuous reduction of around 80-90 % in oxygen concentration at the SWI (C_w=0.1-0.2 C_0=1-2 g m^{-3}) may significantly disturb the growth and metabolism of benthic organisms and can cause mass mortality of marine animals, resulting in benthic defaunation and fish community decline (Diaz and Rosenberg, 1995, and references herein). On the other hand, a turbulent regime promotes high levels of SWI oxygenation.

Oxygen concentration at the SWI can be dynamically driven by periodic fluctuations of the DBL thickness under wind waves and sea swell. Yet the amplitude of these fluctuations during a wave cycle may not be sufficient to stress the benthic macrofauna (around 1 % for C_w/C_0 for instance). In the sediment, periodic fluctuations vanish rapidly and oxygen penetration depth largely depends on the oxygen consumption in the sediment and to a lesser extent, on the wave period in the laminar regime (Fig. 10a) and on the shear velocity in the turbulent regime (Fig. 10b). This sediment inertia is explained by the larger oxygen consumption time (t_c) in the sediment compared to the DBL dynamics time scale during a wave period (t_w). For flows having periods of hours (tides, inertial waves, etc.) or smaller consumption time (*i.e.* smaller C_0, for instance), it can be expected that t_w will reach values comparable to or even larger than t_c. In such cases, periodic fluctuations of oxygen concentration may be expected not only in the overlying water but also in the sediment. However, the fluctuation range as well as the cycle-averaged value are not trivial to extrapolate since a strong coupling between the DBL dynamics, the oxygen diffusion across the DBL, and the oxygen consumption in the sediment is likely to exist when characteristic time scales (t_D, t_c and t_w) have similar orders of magnitude.

Finally, sediment oxygen consumption was modelled using a Michaelis-Menten kinetic formulation. This formulation assumes explicitly that no acclimatization of the respiring community occurs during a wave cycle. Such absence of respiration acclimatization should be tested experimentally as a function of the wave period, for instance with high resolution DO measurements. Although promising results have accompanied the development of optical methods for oxygen concentration profiling (Revsbech et al., 1998), faster oxygen profiles measurements are still required to resolve the temporal dynamics of DO

under wind waves and sea swell. Even the novel non-invasive eddy correlation technique (Berg et al., 2003) requires an integration time of around 150 s, which is still too long to observe high-frequency fluctuations related to high-frequency wave turbulence. Turbulence and diffusion measurements should indeed be measured simultaneously with DO profiles at high-frequency to evaluate the tested model design and the biological interpretations of the mass transfer dynamics at the SWI under periodic waves.

5 Conclusions

The response of dissolved oxygen profiles to a wide range of wind waves to sea swell conditions over a smooth bottom was studied. Oxygen diffusion time across the diffusive boundary layer (t_D), dissolved oxygen uptake (DOU), interfacial concentration (C_w), and oxygen penetration depth (δ_s) were described by their cycle-averaged value and their standard deviation during a wave cycle.

- As in steady flows, the flow regime (turbulent or laminar) controls both the DOU and the oxygen concentration at the SWI. In the laminar regime, oxygen mass transfer efficiency is strongly impeded, yielding small and constant DOU, C_w and δ_s values during the wave cycle. In the turbulent regime (frequent under waves), oxygen supply to the sediment is no longer limited resulting in higher values for $\overline{DOU}$, $\overline{C_w/C_0}$ and δ_s (Fig. 8, Fig. 10a and b).

- In the turbulent regime, DOU and C_w exhibit periodic fluctuations in response to the unsteady DBL thickness: their dynamics were water controlled by the ratio between (a) the diffusion time across the DBL (t_D), and (b) the time allowed for this diffusion during a wave cycle (t_w). When $t_w(t)$ was smaller than $t_D(t)$, the DBL thickness varied more rapidly than the time required for diffusive flux to establish: diffusive flux corresponded to the average DBL thickness over a period. Conversely, when $t_w(t)$ was larger than $t_D(t)$, diffusive flux followed the local DBL thickness fluctuations (Fig. 5). Unsteady properties of the overlying high-frequency flow were never transmitted deeply into the sediment (VAR(δ_s)=0).

- Dependence of the oxygen mass transfer efficiency on the wave period and the orbital velocity are summarized by the non-dimensional Sherwood number (Sh) trends. The latter was found non-dependent on the sediment biogeochemical activity. The cycle-averaged Sherwood values ($\overline{Sh}$) vary little, ranging from 0.17 to 0.23 and with minimum values for sea swells having periods ranging from 10 to 15 s (Fig. 8a). Intra-wave fluctuations VAR(Sh) increase as both wave period and orbital velocity (*i.e.* Reynolds number) increase, ranging from 0.1 % in the laminar regime to 30 % in the turbulent regime (Figs. 8b and **??**b). Finally, although $\overline{Sh}$ values remained lower than values for a steady current with the same maximum shear velocity, high-frequency waves are likely to promote high sediment oxygenation more frequently than steady currents.

Aknowledgements

We would like to thank Jennifer Guarini for correcting the English and for commenting on an earlier version of this paper. The critical remarks of two anonymous reviewers helped to improve the manuscript. This work is a partial fulfillment of the PhD Thesis of Mathieu Chatelain who was supported by a doctoral fellowship from the French National Center for Scientific Research (CNRS).

References

Airy, G. B. (1845). Tides and waves. Encyclopaedia Metropolitana.

Berg, P., Røy, H., Janssen, F., Meyer, V., Jørgensen, B. B., Hüttel, M., and de Beer, D. (2003). Oxygen uptake by aquatic sediments measured with a novel non-invasive eddy-correlation techniqueroy. Marine Ecology Progress Series, 261(1), 75–83.

Berner, R. A. (1980). Early diagenesis: A theoretical approach. Princeton University Press, Princeton.

Booij, K., Sundby, B., and Helder, W. (1994). Measuring the flux of oxygen to a muddy sediment with a cylindrical microcosm. Netherlands Journal of Sea Research, 32, 1–11.

Boudreau, B. P. and Jørgensen, B. B. (2001). The benthic boundary layer: Transport processes and biogeochemistry. Oxford University Press, Oxford.

Butel, R., Dupuis, H., and Bonneton, P. (2002). Spatial variability of wave conditions on the French Atlantic coast using in-situ data. In Proc. ICS, volume 2.

Cai, W.-J. and Sayles, F. L. (1996). Oxygen penetration depths and fluxes in marine sediments. Marine Chemistry, 52(2), 123–131.

Dade, W. (1993). Near-bed turbulence and hydrodynamic control of diffusional mass transfer at the sea floor. Limnology and Oceanography, 38(1), 52–69.

Denny, M. W. (1993). Air and water: The biology and physics of life's media. Princeton University Press, Princeton.

Diaz, R. J. and Rosenberg, R. (1995). Marine benthic hypoxia: A review of its ecological effects and the behavioural responses of benthic macrofauna. Oceanographic Marine Biology Annual Review, 33(1), 245–303.

Dohmen-Janssen, M. (1999). Grain size influence on sediment transport in oscillatory sheet flow. PhD thesis, Delft Technical University.

Fredsøe, J. and Deigaard, R. (1992). Mechanics of coastal sediment transport. Advanced series on ocean engineering, Vol. 3. World Scientific.

Glud, R. N., Berg, P., Fossing, H., and Jørgensen, B. B. (2007). Effect of the diffusive boundary layer on benthic mineralization and O2 distribution: A theoretical model analysis. Limnology and Oceanography, 52(2), 547–557.

Glud, R. N., Gundersen, J. K., Røy, H., and Jørgensen, B. B. (2003). Seasonal dynamics of benthic oxygen uptake in a semienclosed bay: Importance of diffusion and faunal activity. Limnology and Oceanography, 48(3), 1265–1276.

Guizien, K., Dohmen-Janssen, M., and Vittori, G. (2003). 1DV bottom boundary layer modeling under combined wave and current: Turbulent separation and phase lag effects. Journal of Geophysical Research, 108(C1), 3016, doi:10.1029/2001JC001292.

Gundersen, J. K. and Jørgensen, B. B. (1990). Microstructure of diffusive boundary layers and the oxygen uptake of the sea floor. Nature, 345(6276), 604–607.

Hao, O. F., Richard, M. G., Jenkins, D., and Blanch, H. W. (1983). The half-saturation coefficient for dissolved oxygen: A dynamic method for its determination and its effect on dual species competition. Biotechnology and Bioengineering, 25(1), 403–416.

Harris, P. T. and Coleman, R. (1998). Estimating global shelf sediment mobility due to swell waves. Marine Geology, 150(1-4), 171–177.

Higashino, M., Gantzer, C. J., and Stefan, H. G. (2004). Unsteady diffusional mass transfer at the sediment/water interface: Theory and significance for SOD measurement. Water Research, 38(1), 1–12.

Higashino, M., Stefan, H. G., and Gantzer, C. J. (2003). Periodic diffusional mass transfer near sediment/water interface: Theory. Journal of Environmental Engineering, 129(5), 447–455.

Hondzo, M. (1998). Dissolved oxygen transfer at the sediment-water interface in a turbulent flow. Water Resources Research, 34(12), 3525–3533.

House, W. A. (2003). Factors influencing the extent and development of the oxic zone in sediments. Biogeochemistry, 63(3), 317–334.

Jensen, B. L., Sumer, B. M., and Fredsøe, J. (2006). Turbulent oscillatory boundary layers at high Reynolds numbers. Journal of Fluid Mechanics, 206(1), 265–297.

Jørgensen, B. B. and Des Marais, D. J. (1990). The diffusive boundary layer of sediments: Oxygen microgradients over a microbial mat. Limnology and Oceanography, 35(6), 1343–1355.

Jørgensen, B. B. and Revsbech, N. P. (1985). Diffusive boundary layers and the oxygen uptake of sediments and detritus. Limnology and Oceanography, 30(1), 111–122.

Llansó, R. J. (1992). Effects of hypoxia on estuarine benthos: The lower Rappahannock River (Chesapeake Bay), a case study. Estuarine, Coastal and Shelf Science, 35(5), 491–515.

Lohse, L., Epping, E. H., Helder, W., and Van Raaphorst, W. (1996). Oxygen pore water profiles in continental shelf sediments of the North Sea: Turbulent versus molecular diffusion. Marine Ecology Progress Series, 145(1), 63–75.

Lorke, A., Müller, B., Maerki, M., and Wüest, A. (2003). Breathing sediments: The control of diffusive transport across the sediment-water interface by periodic boundary-layer turbulence. Limnology and Oceanography, 48(6), 2077–2085.

Mackenthun, A. A. and Stefan, H. G. (1998). Effect of flow velocity on sediment oxygen demand: Experiments. Journal of Environmental Engineering, 124, 222–230.

Manheim, F. T. and Waterman, L. S. (1974). Diffusimetry (diffusion constant estimation) on sediment cores by resistivity probe. Initial Reports of Deep-Sea Drilling Project, 22(1), 663–670.

Massel, S. R. (1996). Ocean surface waves. Their physics and prediction. World Scientific.

Nakamura, Y. and Stefan, H. G. (1994). Effect of flow velocity on sediment oxygen demand: Theory. Journal of Environmental Engineering, 120(5), 996–1016.

Patankar, S. V. (1980). Numerical heat transfer and fluid flow. MacGraw-Hill, New-York.

Proudman, J. (1953). Dynamical Oceanography. Methuen London and Wiley, New-York.

Rahm, L. and Svensson, U. (1989). On the mass transfer properties of the benthic boundary layer with an application to oxygen fluxes. Netherlands Journal of Sea Research, 24(1), 27–35.

Revsbech, N. P., Nielsen, L. P., and Ramsing, N. B. (1998). A novel microsensor for determination of apparent diffusivity in sediments. Limnology and Oceanography, 43(5), 986–992.

Steinberger, N. and Hondzo, M. (1999). Diffusional mass transfer at sediment-water interface. Journal of Environmental Engineering, 125(2), 192–200.

Tengberg, A., Stahl, H., Gust, G., Muller, V., Arning, U., Andersson, H., and Hall, P. O. J. (2004). Intercalibration of benthic fluxes chambers I. Accuracy of flux measurements and influence of chamber hydrodynamics. 60, 1–28.

Ullman, W. J. and Aller, R. C. (1982). Diffusion coefficients in nearshore marine sediments. Limnology and Oceanography, 27(3), 552–556.

Vittori, G. and Verzicco, R. (1998). Direct simulation of transition in an oscillatory boundary layer. Journal of Fluid Mechanics, 37, 207–232.

List of Figures

A Symbols

Symbol	Unit	Description
C	$[\mathrm{M}].[\mathrm{L}]^{-3}$	Dissolved oxygen concentration
C_0	$[\mathrm{M}].[\mathrm{L}]^{-3}$	Bulk water concentration
C_w	$[\mathrm{M}].[\mathrm{L}]^{-3}$	Interfacial concentration
D	$[\mathrm{L}]^2.[\mathrm{T}]^{-1}$	Vertical diffusivity
DOU	$[\mathrm{M}].[\mathrm{L}]^2.[\mathrm{T}]^{-1}$	Dissolved oxygen uptake
D_s	$[\mathrm{L}]^2.[\mathrm{T}]^{-1}$	Effective diffusivity
D_t	$[\mathrm{L}]^2.[\mathrm{T}]^{-1}$	Turbulent diffusivity
D_w	$[\mathrm{L}]^2.[\mathrm{T}]^{-1}$	Molecular diffusivity
d_{50}	[L]	Median diameter of the sediment grain
h	[L]	Length of the computational grid ($=h_w+h_s$)
h_w	[L]	Modelled water height
h_s	[L]	Modelled sediment depth
k_n	[L]	Bottom roughness
K_{O_2}	$[\mathrm{M}].[\mathrm{L}]^{-3}$	Dissolved oxygen half-saturation constant
m	-	Numerical constant
n_s	-	Number of computational points in sediment
n_w	-	Number of computational points in water
n_t	-	Number of time steps that defines a period
Re_δ	-	Reynolds number
Sc	-	Schmidt number
Sh	-	Sherwood number
r, s	-	Constants for grid definition
t	[T]	Time
t_c	[T]	Consumption time in sediment
t_D	[T]	Diffusion time across diffusive boundary layer
t_{st}	[T]	Convergence time of the computations
T	[T]	Wave period
u^*	$[\mathrm{L}].[\mathrm{T}]^{-1}$	Bottom shear velocity
u^*_m	$[\mathrm{L}].[\mathrm{T}]^{-1}$	Maximum shear velocity
U	$[\mathrm{L}].[\mathrm{T}]^{-1}$	Wave velocity
U_w	$[\mathrm{L}].[\mathrm{T}]^{-1}$	Nearbed orbital velocity of the flow
z	[L]	Y-coordinate (positive upward)
α	-	Numerical constant
β	$[\mathrm{L}]^4$	Slope of oxygen profile at sediment-water interface
δ	[L]	Wave viscous boundary layer height (Stokes length)
δ_D	[L]	Diffusive boundary layer thickness
δ_ν	[L]	Viscous sublayer thickness
δ_s	[L]	Oxygen penetration depth
ϵ	-	Convergence criterion
μ	$[\mathrm{M}].[\mathrm{L}]^{-3}.[\mathrm{T}]^{-1}$	Biogeochemical activity of the sediment
ν	$[\mathrm{L}]^2.[\mathrm{T}]^{-1}$	Kinematic viscosity in water
ν_t	$[\mathrm{L}]^2.[\mathrm{T}]^{-1}$	Eddy viscosity of the fluid
ϕ	-	Sediment porosity
φ	$[^o\mathrm{C}]$	Wave phase
ρ	$[\mathrm{M}].[\mathrm{L}]^{-3}$	Water density
τ	$[\mathrm{M}].[\mathrm{L}]^{-1}.[\mathrm{T}]^{-2}$	Bottom shear stress

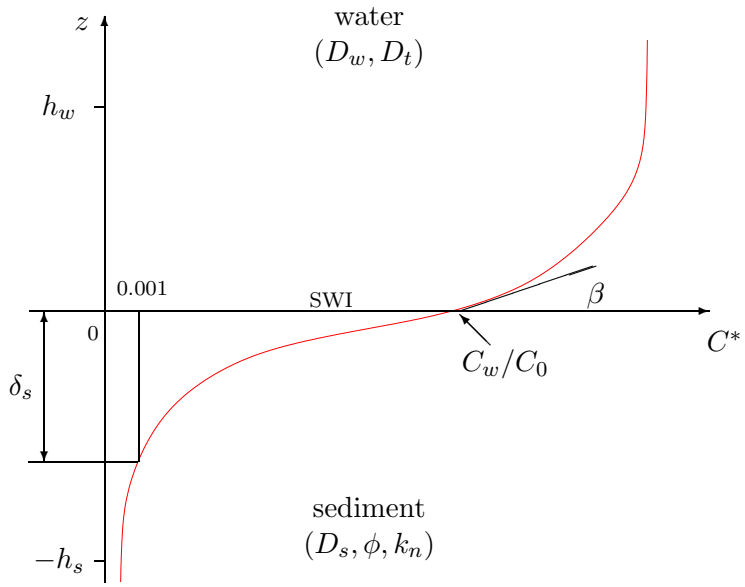

Figure 1: Schematic representation of non-dimensional dissolved oxygen concentration profile (C^*=C/C_0) at the sediment-water interface (SWI).

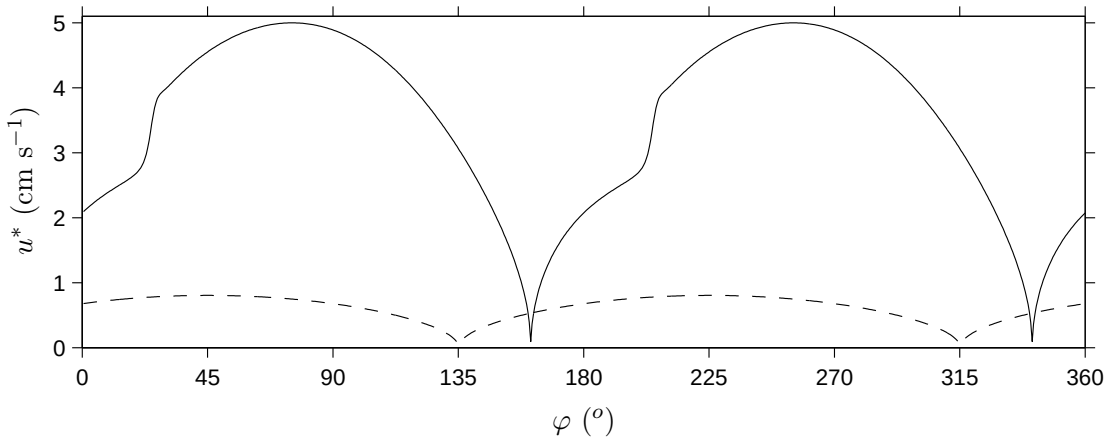

Figure 2: Shear velocity u^* during a wave cycle for T=15 s, and u^*_m=5 cm s^{-1} (solid line), u^*_m=0.8 cm s^{-1} (dashed line).

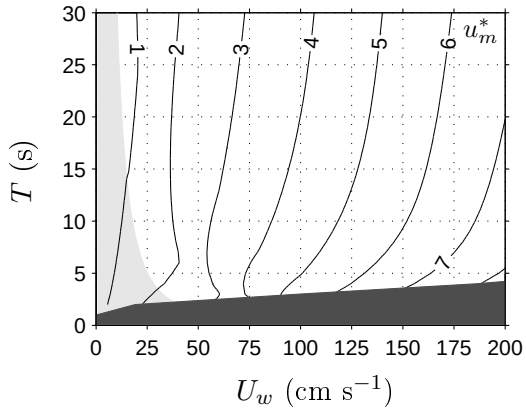

Figure 3: Maximum shear velocity u_m^* dependence on orbital velocity U_w and period T of the wave. Dark grey delimits the unstable breaking waves ($H < 0.8\ D$) and light grey delimits the laminar regime ($Re_\delta < 320$).

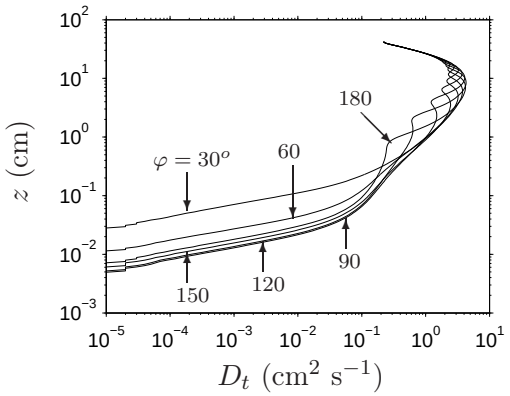

Figure 4: Vertical profiles of turbulent diffusivity D_t at different wave phases φ, for u_m^*=5 cm s^{-1} and T=25 s.

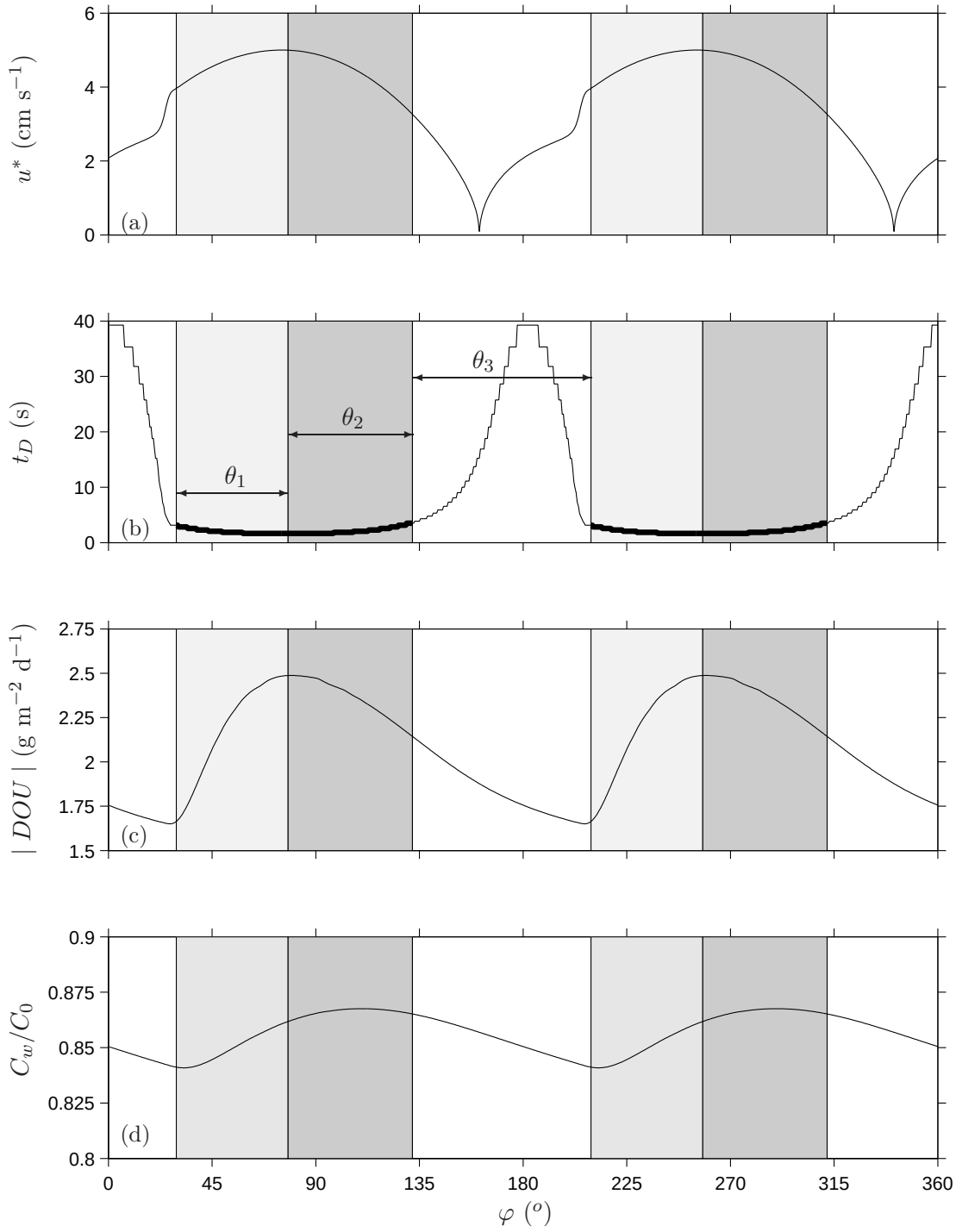

Figure 5: Temporal evolution of (a) u^*, (b) t_D, (c) DOU, and (d) C_w/C_0 during a wave cycle, for u^*_m=5 cm s^{-1}, T=15 s, and μ=2000 g m^{-3} d^{-1}. Light grey delimits the turbulent period θ_1 and dark grey delimits the turbulent period θ_2.

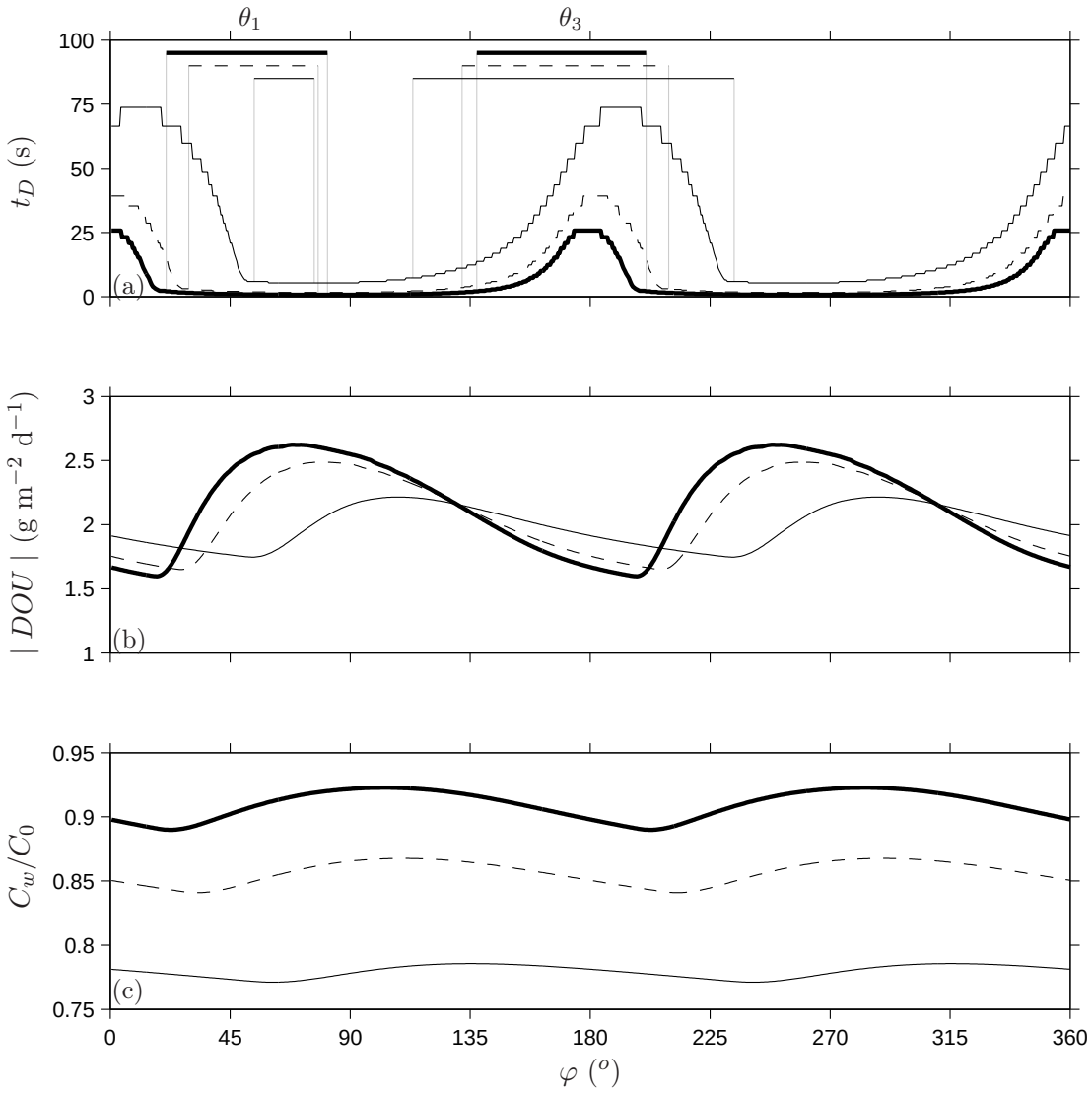

Figure 6: Temporal evolution of (a) t_D, (b) DOU, and (c) C_w/C_0 during a wave cycle, for T=15 s, μ=2000 g m^{-3} d^{-1}, and u_m^*=3 cm s^{-1} (solid line), u_m^*=5 cm s^{-1} (dashed line), u_m^*=7 cm s^{-1} (bold line).

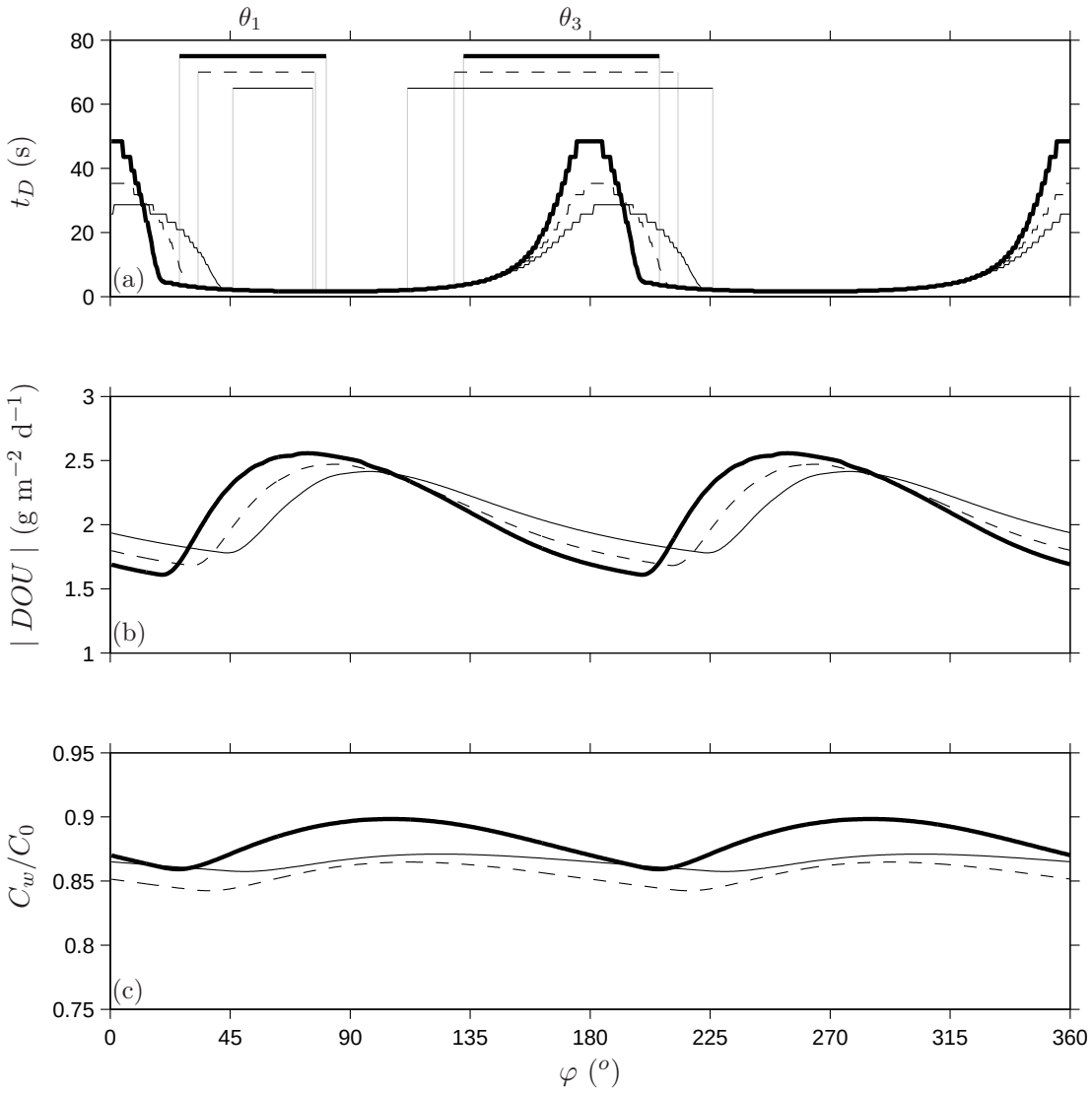

Figure 7: Temporal evolution of (a) t_D, (b) DOU, and (c) C_w/C_0 during a wave cycle, for u_m^*=5 cm s^{-1}, μ=2000 g m^{-3} d^{-1}, and T=7 s (solid line), T=12 s (dashed line), T=25 s (bold line).

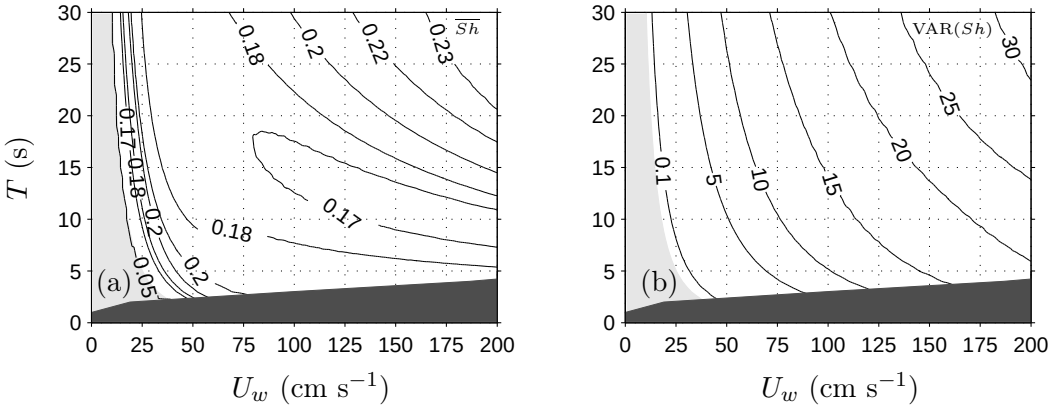

Figure 8: Isograms of (a) $\overline{Sh}$, and (b) VAR(Sh) showing dependences on orbital velocity U_w and wave period T. Dark grey delimits the unstable breaking waves ($H < 0.8\ D$) and light grey delimits the laminar regime ($Re_\delta < 320$).

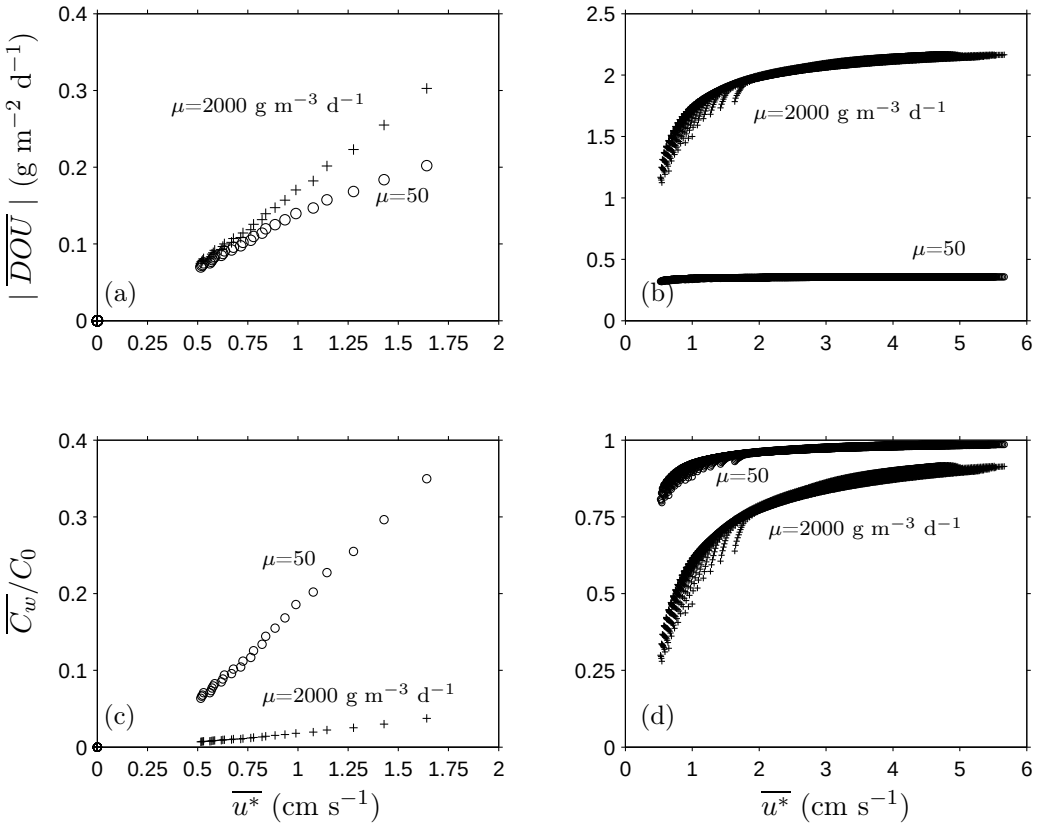

Figure 9: Dependences of $\overline{DOU}$ (a,b) and $\overline{C_w}/C_0$ (c,d) on cycle-averaged shear velocity $\overline{u^*}$ for two biogeochemical activities. (a,c) are for the laminar regime ($Re_\delta < 320$), (b,d) are for the turbulent regime ($Re_\delta > 320$).

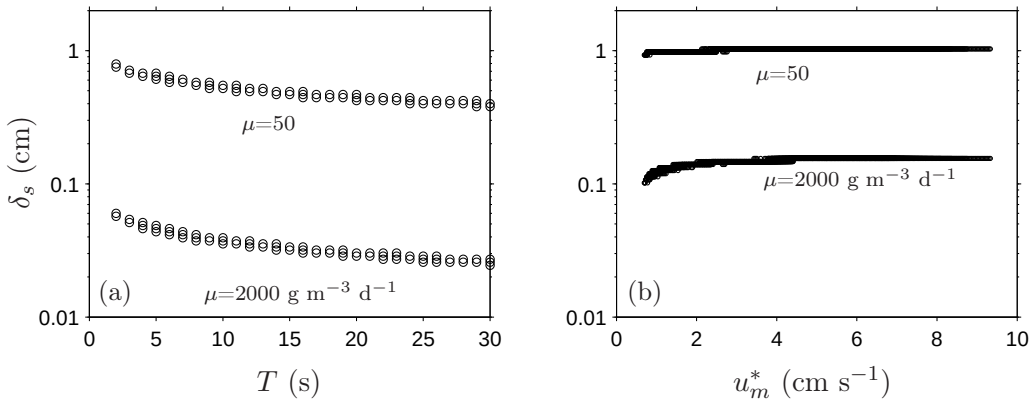

Figure 10: Penetration depth δ_s dependence on (a) wave period T for the laminar regime ($Re_\delta \leq$320) and (b) maximum shear velocity u_m^* for the turbulent regime ($Re_\delta >$320), and the two biogeochemical activities tested.